TECHNICAL RESEARCH REPORT

Sampled-Data Modeling and Analysis of PWM DC-DC Converters Under Hysteretic Control

by C.-C. Fang, E.H. Abed

T.R. 98-56

Report Documentation Page

Form Approved
OMB No. 0704-0188

1. REPORT DATE	2. REPORT TYPE	3. DATES COVERED
1998		**-**

4. TITLE AND SUBTITLE	5a. CONTRACT NUMBER
Sampled-Data Modeling and Analysis of PWM DC-DC Converters Under Hysteretic Control	5b. GRANT NUMBER
	5c. PROGRAM ELEMENT NUMBER
6. AUTHOR(S)	5d. PROJECT NUMBER
	5e. TASK NUMBER
	5f. WORK UNIT NUMBER
7. PERFORMING ORGANIZATION NAME(S) AND ADDRESS(ES) **Office of Naval Research,One Liberty Center,875 North Randolph Street Suite 1425,Arlington,VA,22203-1995**	8. PERFORMING ORGANIZATION REPORT NUMBER
9. SPONSORING/MONITORING AGENCY NAME(S) AND ADDRESS(ES)	10. SPONSOR/MONITOR'S ACRONYM(S)
	11. SPONSOR/MONITOR'S REPORT NUMBER(S)

12. DISTRIBUTION/AVAILABILITY STATEMENT
Approved for public release; distribution unlimited

13. SUPPLEMENTARY NOTES

14. ABSTRACT
see report

15. SUBJECT TERMS

16. SECURITY CLASSIFICATION OF:			17. LIMITATION OF ABSTRACT	18. NUMBER OF PAGES	19a. NAME OF RESPONSIBLE PERSON
a. REPORT	b. ABSTRACT	c. THIS PAGE			
unclassified	**unclassified**	**unclassified**		**12**	

Sampled-Data Modeling and Analysis of PWM DC-DC Converters Under Hysteretic Control

Chung-Chieh Fang and Eyad H. Abed
Department of Electrical Engineering
and the Institute for Systems Research
University of Maryland
College Park, MD 20742 USA

Manuscript: September 28, 1998

Abstract

The PWM DC-DC converter in continuous conduction mode under hysteretic control is modeled and analyzed using the sampled-data approach. This work complements other recent work of the authors on sampled-data modeling and analysis of PWM converters, where the focus was on fixed switching frequency operation. Nonlinear and linearized sampled-data models, and the control-to-output transfer function are derived. The analysis is exact if the source and reference signals are constant (or constant within each cycle).

1 Introduction

The PWM DC-DC converter in continuous conduction mode under hysteretic control is modeled and analyzed using the sampled-data approach. This work complements other recent work of the authors on sampled-data modeling and analysis of PWM converters [1, 2], where the focus was on fixed switching frequency operation. Since the switching frequency is variable in hysteretic control, there are steps in the modeling process which differ from the corresponding steps in the modeling of fixed switching frequency operation. In the sampled-data approach, the analysis is exact if the source and reference signals are constant (or constant within each cycle). Besides being accurate, the approach presented here is systematic and can be applied to other types of variable frequency control (e.g. constant-on-time, constant-off-time, etc.).

Previous works [3, 4, 5] on modeling and analysis of PWM DC-DC converters under hysteretic control are generally based on the averaging method. The advantage of the sampled-data approach

is that it is more accurate, in that it involves detailed modeling of behavior between switching instants.

The organization of the paper is as follows. In Sec. 2, a general block diagram model for a PWM converter under hysteretic control is proposed. In Sec. 3, a nonlinear sampled-data model is derived. Linearized sampled-data dynamics near a fixed point is derived in Sec. 4. In Sec. 5, the control-to-output transfer function, the audio-susceptibility, and the output impedance are derived. In Sec. 6, an illustrative example is given. Conclusions are given in Sec. 7.

2 Block Diagram Model

A general block diagram model of a PWM converter in continuous conduction mode (CCM) under hysteretic control is given in Fig. 1, where the functioning of switching decision box is shown in Fig. 2. In the diagram, $A_1, A_2 \in \mathbf{R}^{N\times N}$, $B_1, B_2 \in \mathbf{R}^{N\times 1}$, and $C, E_1, E_2 \in \mathbf{R}^{1\times N}$ are constant matrices, $x \in \mathbf{R}^N$, $y \in \mathbf{R}$ are the state and the feedback signal, respectively. The source voltage is v_s; the output voltage is v_o. The notation v_r denotes the reference signal, which could be a voltage or current reference. The signal v_r can also be used as a control variable. In this case, Fig. 1 can be viewed as a power stage.

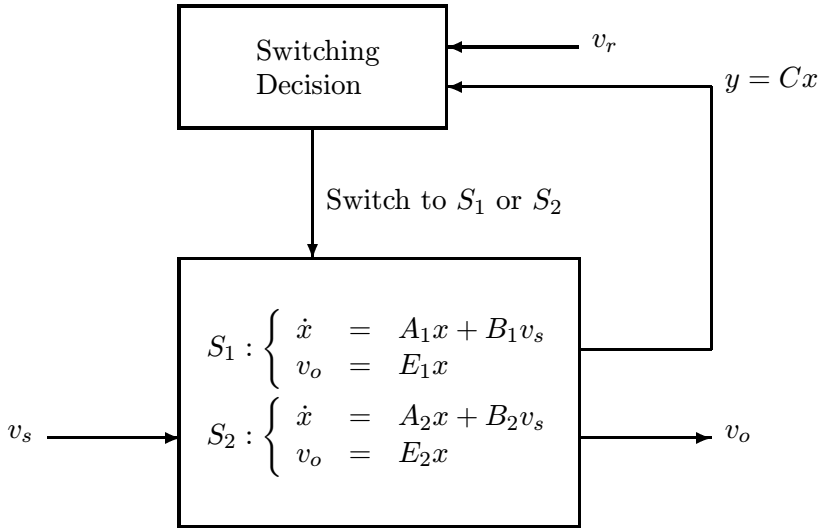

Figure 1: A general model for PWM converters in CCM under hysteretic control

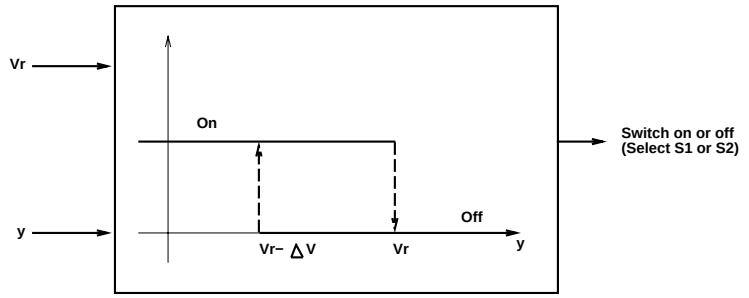

Figure 2: The switching decision box in Fig. 1

The hysteretic control operation is as follows: When $y < v_r$, the controlled switch is turned on. The switch is turned off when $y = v_r$ (the reference value), and it is turned on again when $y = v_r - \Delta V$ (where ΔV is a given constant). Thus the duration of an on-off cycle is variable.

3 Nonlinear Sampled-Data Model

Consider the dynamics of the PWM converter of Fig. 1 within the n-th cycle. Let the duration of the n-th cycle be T_n, and let the time at the beginning of the n-th cycle be $t_n = \sum_{i=0}^{n-1} T_i$. Generally in the PWM converter, the switching frequency is sufficiently high that the variations in v_s and v_r in a cycle can be neglected. Thus, take v_s and v_r to be constant within the cycle, with values denoted by v_{sn} and v_{rn}, respectively. Denote by $t_n + d_n$ the switching instant within the cycle when the switch is turned off. It follows that

$$y(t_n + d_n) = Cx(t_n + d_n) = v_{rn} \tag{1}$$

$$y(t_n + T_n) = Cx_{n+1} = v_{rn} - \Delta V \tag{2}$$

and the dynamics within the two stages S_1 and S_2 are given by

$$S_1 : \begin{cases} \dot{x} = A_1 x + B_1 v_s \\ v_o = E_1 x \end{cases} \quad \text{for } t \in [t_n, t_n + d_n) \tag{3}$$

$$S_2 : \begin{cases} \dot{x} = A_2 x + B_2 v_s \\ v_o = E_2 x \end{cases} \quad \text{for } t \in [t_n + d_n, t_n + T_n) \tag{4}$$

To develop a sampled-data model from the description above, sample the state x at times t_n,

noting from the definition of t_n that $t_{n+1} = t_n + T_n$. Figure 3 illustrates the mapping taking x_n, the state at time t_n, to $x_{n+1} = x(t_{n+1}) = x(t_n + T_n)$.

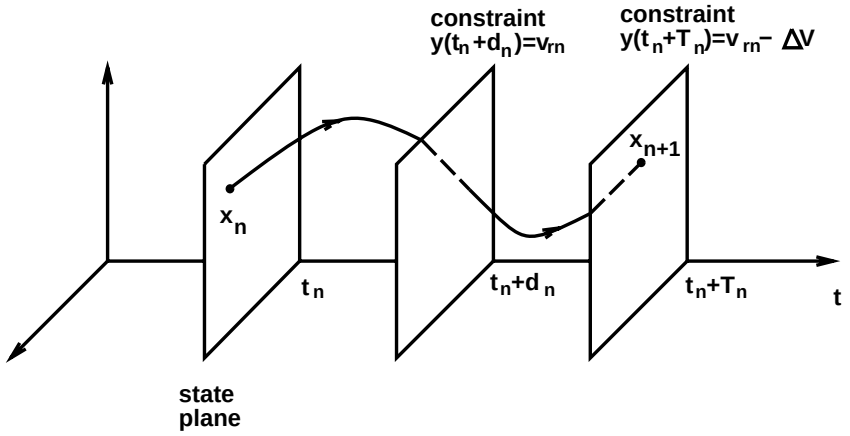

Figure 3: Illustration of sampled-data dynamics of PWM converter in CCM with hysteretic control

The role of Eqs. (1) and (2) require some explanation. Eq. (1) defines the time interval d_n after the start of a cycle at which switching from stage S_1 to stage S_2 occurs. Since the state is sampled at times t_n and not at intermediate switching times $t_n + d_n$, this equation does not constrain the state. On the other hand, Eq. (2) both defines a switching time (namely T_n) and imposes a constraint on the state.

From Eqs. (1)-(4), the PWM converter in CCM under hysteretic control has the following sampled-data dynamics (here $\tau_n := (d_n, T_n)'$):

$$\begin{aligned} x_{n+1} &= f(x_n, v_{sn}, \tau_n) \\ &= e^{A_2(T_n - d_n)}(e^{A_1 d_n} x_n + \int_0^{d_n} e^{A_1 \sigma} d\sigma B_1 v_{sn}) + \int_0^{T_n - d_n} e^{A_2 \sigma} d\sigma B_2 v_{sn} \qquad (5) \\ v_o &= E x_n \qquad (6) \end{aligned}$$

with the constraint equation

$$\begin{aligned} & g(x_n, v_{sn}, \tau_n, v_{rn}) \\ &= \begin{bmatrix} y(t_n + d_{1n}) - v_{rn} \\ y(t_n + T_n) - v_{rn} + \Delta V \end{bmatrix} \end{aligned}$$

$$= \begin{bmatrix} C(e^{A_1 d_n} x_n + \int_0^{d_n} e^{A_1 \sigma} d\sigma B_1 v_{sn}) - v_{rn} \\ C(e^{A_2(T_n - d_n)}(e^{A_1 d_n} x_n + \int_0^{d_n} e^{A_1 \sigma} d\sigma B_1 v_{sn}) + \int_0^{T_n - d_n} e^{A_2 \sigma} d\sigma B_2 v_{sn}) - v_{rn} + \Delta V \end{bmatrix}$$

$$= 0 \tag{7}$$

(As in [1, 2], E is used to denote E_1, E_2, or $(E_1+E_2)/2$ depending on which value of output voltage is of interest: E_1 is used if the output voltage is sampled at the start of the cycle; E_2 if the output voltage is sampled at the end of the preceding cycle; and $(E_1 + E_2)/2$ if the average of these two is used.)

Since Eq. (2) places a constraint on the state, the dynamics is actually $(N-1)$-dimensional rather than N-dimensional.

The fixed point $(x_n, v_{sn}, \tau_n, v_{rn}) = (x^0(0), V_s, (d,T)', V_r)$ satisfies

$$x^0(0) = f(x^0(0), V_s, (d,T)') \tag{8}$$

$$g(x^0(0), V_s, (d,T)', V_r) = 0 \tag{9}$$

Given the values of V_s and V_r, these $N+2$ nonlinear equations in $N+2$ unknowns ($x^0(0)$, d and T) can be solved by Newton's method.

4 Linearized Sampled-Data Dynamics

Linearizing the dynamics (5)-(7) at the fixed point $(x^0(0), V_s, (d,T)', V_r)$ and using $\diamond$ to denote evaluation at that point, it follows that

$$\begin{array}{rcl} \hat{x}_{n+1} & \approx & \Phi_h \hat{x}_n + \Gamma_{hv} \hat{v}_{sn} + \Gamma_{hr} \hat{v}_{rn} \\ \hat{v}_{on} & = & E \hat{x}_n \end{array} \tag{10}$$

where

$$\Phi_h = \frac{\partial f}{\partial x_n} - \frac{\partial f}{\partial \tau_n} (\frac{\partial g}{\partial \tau_n})^{-1} \frac{\partial g}{\partial x_n} \Big|_\diamond \tag{11}$$

$$\Gamma_{hv} = \frac{\partial f}{\partial v_{sn}} - \frac{\partial f}{\partial \tau_n} (\frac{\partial g}{\partial \tau_n})^{-1} \frac{\partial g}{\partial v_{sn}} \Big|_\diamond \tag{12}$$

$$\Gamma_{hr} = -\frac{\partial f}{\partial \tau_n} (\frac{\partial g}{\partial \tau_n})^{-1} \frac{\partial g}{\partial v_{rn}} \Big|_\diamond \tag{13}$$

$$\left.\frac{\partial f}{\partial x_n}\right|_{\diamond} = e^{A_2(T-d)}e^{A_1 d} \tag{14}$$

$$\left.\frac{\partial f}{\partial \tau_n}\right|_{\diamond} = \left[\begin{array}{cc} e^{A_2(T-d)}((A_1-A_2)x^0(d)+(B_1-B_2)) & A_2x^0(T)+B_2V_s \end{array}\right] \tag{15}$$

$$= \left[\begin{array}{cc} e^{A_2(T-d)}(\dot{x}^0(d^-)-\dot{x}^0(d^+)) & \dot{x}^0(T^-) \end{array}\right] \tag{16}$$

$$\left.\frac{\partial g}{\partial \tau_n}\right|_{\diamond} = \left[\begin{array}{cc} C\dot{x}^0(d^-) & 0 \\ Ce^{A_2(T-d)}(\dot{x}^0(d^-)-\dot{x}^0(d^+)) & C\dot{x}^0(T^-) \end{array}\right] \tag{17}$$

$$\left.\frac{\partial g}{\partial x_n}\right|_{\diamond} = \left[\begin{array}{c} C \\ Ce^{A_2(T-d)} \end{array}\right] e^{A_1 d} \tag{18}$$

$$\left.\frac{\partial f}{\partial v_{sn}}\right|_{\diamond} = e^{A_2(T-d)}\int_0^d e^{A_1\sigma}d\sigma B_1 + \int_0^{T-d} e^{A_2\sigma}d\sigma B_2 \tag{19}$$

$$\left.\frac{\partial g}{\partial v_{sn}}\right|_{\diamond} = \left[\begin{array}{c} C\int_0^d e^{A_1\sigma}d\sigma B_1 \\ C(e^{A_2(T-d)}\int_0^d e^{A_1\sigma}d\sigma B_1 + \int_0^{T-d} e^{A_2\sigma}d\sigma B_2) \end{array}\right] \tag{20}$$

$$\left.\frac{\partial f}{\partial v_{rn}}\right|_{\diamond} = 0 \tag{21}$$

$$\left.\frac{\partial g}{\partial v_{rn}}\right|_{\diamond} = \left[\begin{array}{c} -1 \\ -1 \end{array}\right] \tag{22}$$

Although as noted above the dynamics are reality $(N-1)$-dimensional, Eq. (10) is an N-dimensional model. Thus there is an eigenvalue of Φ_h at 0, implying $\det[\Phi_h]=0$. For completeness, an analytical proof of this fact is given:

$$\begin{aligned}\det[\Phi_h] &= \det[e^{A_2(T-d)}(I - \left[\begin{array}{cc} \dot{x}^0(d^-)-\dot{x}^0(d^+) & \dot{x}^0(d^+) \end{array}\right](\frac{\partial g}{\partial \tau_n})^{-1}\Big|_{\diamond}\cdot \\ &\quad \left[\begin{array}{c} C \\ Ce^{A_2(T-d)} \end{array}\right])e^{A_1 d}] \\ &= \det[e^{A_1 d}e^{A_2(T-d)}]\det[I - \left[\begin{array}{cc} \dot{x}^0(d^-)-\dot{x}^0(d^+) & \dot{x}^0(d^+) \end{array}\right](\frac{\partial g}{\partial \tau_n})^{-1}\Big|_{\diamond}\cdot \\ &\quad \left[\begin{array}{c} C \\ Ce^{A_2(T-d)} \end{array}\right]]\end{aligned}$$

$$
\begin{aligned}
&= \det[e^{A_1 d} e^{A_2(T-d)}]\det[I - \left[\begin{array}{c} C \\ Ce^{A_2(T-d)} \end{array}\right] \left[\begin{array}{cc} \dot{x}^0(d^-) - \dot{x}^0(d^+) & \dot{x}^0(d^+) \end{array}\right] \cdot \\
&\quad \frac{\left[\begin{array}{cc} C\dot{x}^0(T^-) & 0 \\ Ce^{A_2(T-d)}(\dot{x}^0(d^+) - \dot{x}^0(d^-)) & C\dot{x}^0(d^-) \end{array}\right]}{C\dot{x}^0(d^-)C\dot{x}^0(T^-)}] \\
&= \det[e^{A_1 d} e^{A_2(T-d)}]\det[\left[\begin{array}{cc} \frac{C\dot{x}^0(d^+)Ce^{A_2(T-d)}\dot{x}^0(d^-)}{C\dot{x}^0(d^-)C\dot{x}^0(T^-)} & \frac{C\dot{x}^0(d^+)}{C\dot{x}^0(T^-)} \\ 0 & 0 \end{array}\right]] \\
&= 0
\end{aligned}
$$

The system in Fig. 1 is asymptotically stable if all of the eigenvalues of Φ_h are inside the unit circle of the complex plane. The transient response towards the periodic orbit $x^0(t)$ is determined by the magnitudes of the eigenvalues.

5 Control-to-Output Transfer Function, Audio-Susceptibility and Output Impedance

From Eq. (10), the control (v_r) to output transfer function and audio-susceptibility are, respectively,

$$T_{oc}(z) = \frac{\hat{v}_o(z)}{\hat{v}_r(z)} = E(zI - \Phi_h)^{-1}\Gamma_{hr} \tag{23}$$

$$T_{os}(z) = \frac{\hat{v}_o(z)}{\hat{v}_s(z)} = E(zI - \Phi_h)^{-1}\Gamma_{hv} \tag{24}$$

To calculate the output impedance, add a fictitious current source i_o (as a perturbation) in parallel with the load. Then the dynamical equations describing the dynamics within each stage Eqs. (3) and (4) are replaced by

$$S_1 : \dot{x} = A_1 x + B_1 v_s + B_{i1} i_o \tag{25}$$

$$S_2 : \dot{x} = A_2 x + B_2 v_s + B_{i2} i_o \tag{26}$$

Since i_o is used as perturbation, the nominal value of i_o is 0. Similar to the derivation of

audio-susceptibility, the output impedance is

$$T_{oo}(z) = \frac{\hat{v}_o(z)}{\hat{i}_o(z)} = E(zI - \Phi_h)^{-1}\Gamma_{hi} \tag{27}$$

where

$$\Gamma_{hi} = \frac{\partial f}{\partial i_{on}} - \frac{\partial f}{\partial \tau_n}(\frac{\partial g}{\partial \tau_n})^{-1}\frac{\partial g}{\partial i_{on}}\Big|_\diamond \tag{28}$$

$$\frac{\partial f}{\partial i_{on}}\Big|_\diamond = e^{A_2(T-d)}\int_0^d e^{A_1\sigma}d\sigma B_{i1} + \int_0^{T-d} e^{A_2\sigma}d\sigma B_{i2} \tag{29}$$

$$\frac{\partial g}{\partial i_{on}}\Big|_\diamond = \begin{bmatrix} C\int_0^d e^{A_1\sigma}d\sigma B_{i1} \\ C(e^{A_2(T-d)}\int_0^d e^{A_1\sigma}d\sigma B_{i1} + \int_0^{T-d} e^{A_2\sigma}d\sigma B_{i2}) \end{bmatrix} \tag{30}$$

and $\diamond$ denotes the evaluation at $(x_n, v_{sn}, \tau_n, v_{rn}, i_{on}) = (x^0(0), V_s, (d,T)', V_r, 0)$.

6 Illustrative Example

The results of the paper are now applied to the boost converter under hysteretic control studied in [5]. The system diagram is shown in Fig. 4, where $R = 10\Omega$, $L = 290\mu H$, $C = 760\mu F$, $V_s = 10V$, $V_r = 4A$ (current reference) and $\Delta V = 0.1A$.

Let the system state be $x = (i_L, v_C)$. The matrices in the block diagram model of Fig. 1 are

$$A_1 = \begin{bmatrix} 0 & 0 \\ 0 & \frac{-1}{RC} \end{bmatrix}$$

$$A_2 = \begin{bmatrix} 0 & \frac{-1}{L} \\ \frac{1}{C} & \frac{-1}{RC} \end{bmatrix}$$

$$B_1 = B_2 = \begin{bmatrix} \frac{1}{L} \\ 0 \end{bmatrix}$$

$$C = \begin{bmatrix} 1 & 0 \end{bmatrix}$$

$$E_1 = E_2 = \begin{bmatrix} 0 & 1 \end{bmatrix}$$

The fixed point is calculated as $(x^0(0), V_s, (d_n, T_n)', V_r) = ((3.9000; 19.8784)', 10, (2.9\times10^{-6}, 5.8368\times 10^{-6})', 4)$.

Because of the simplicity of the on stage in the boost converter, the constraint equation (7) can be further simplified to

$$\begin{aligned} & g(x_n, v_{sn}, \tau_n, v_{rn}) \\ = & \left[\begin{array}{c} L\frac{\Delta V}{d_n} - v_{sn} \\ C(e^{A_2(T_n-d_n)}(e^{A_1 d_n}x_n + \int_0^{d_n} e^{A_1\sigma}d\sigma B_1 v_{sn}) + \int_0^{T_n-d_n} e^{A_2\sigma}d\sigma B_2 v_{sn}) - v_{rn} + \Delta V \end{array} \right] \\ = & \ 0 \end{aligned} \tag{31}$$

From Eq. (11), it follows that

$$\Phi_h = e^{A_2(T-d)}(I - \frac{\dot{x}^0(d^+)Ce^{A_2(T-d)}}{Ce^{A_2(T-d)}\dot{x}^0(d^+)})e^{A_1 d} \tag{32}$$

Also,

$$\det[\Phi_h] = \det[e^{A_1 d}e^{A_2(T-d)}](1 - \frac{Ce^{A_2(T-d)}\dot{x}^0(d^+)}{Ce^{A_2(T-d)}\dot{x}^0(d^+)}) = 0$$

Thus one pole is 0 and the sampled-data dynamics is 1-dimensional. The other pole obtained directly from $\sigma[\Phi_h]$ is 0.9985. This pole can also be analytically approximated (using a technique discussed in [6, Chapter 6]) as

$$1 + \frac{(T-d)(R(V_r - \Delta V) - v_C^0(0))}{RC(V_s - v_C^0(0))} \tag{33}$$

Using this formula, the estimated pole is 0.9993, which is very close to the exact value obtained directly from $\sigma[\Phi_h]$. The magnitude of this eigenvalue is very close to 1, indicating a slow transient to the *periodic orbit*. This does not contradict the fact, observed in [5], that the inductor current is quickly captured in the range between $3.9A$ and $4A$.

The control (v_r) to output transfer function $E(zI - \Phi_h)^{-1}\Gamma_{hr}$ was calculated and an unstable zero was found at 1.0537. This will cause an undershoot in the output voltage for a step change in v_r. The associated frequency response is shown in Fig. 5. These results agree very well with [5].

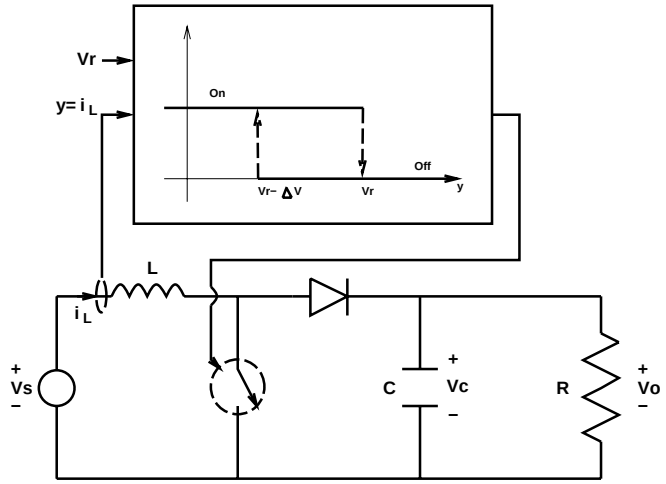

Figure 4: System diagram for a boost converter under hysteretic control

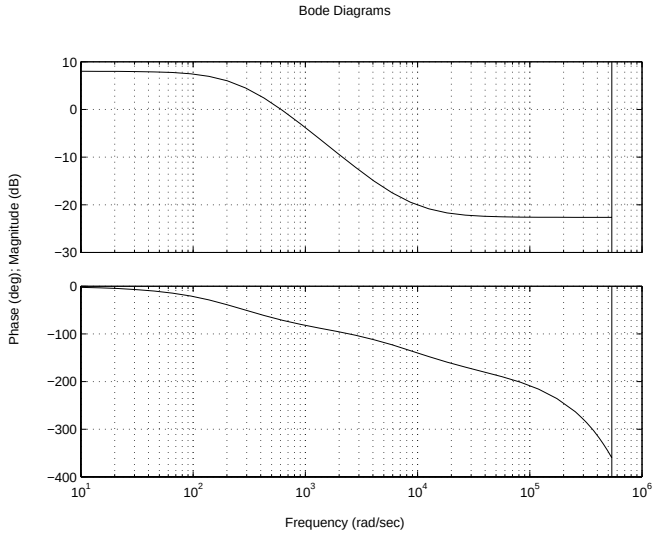

Figure 5: Control-to-output frequency response

7 Concluding Remarks

Sampled-data models and associated analysis have been developed for the PWM DC-DC converter in continuous conduction mode under hysteretic control. The main distinguishing feature of this work in comparison with the authors' papers [1, 2] is the presence of a variable switching frequency. Nonlinear and linearized sampled-data models, the control-to-output transfer function, audio-susceptibility, and output impedance have been derived. The sampled-data approach employed is systematic and can be used under general conditions. The analysis is exact if the source and reference voltage signals are constant (or constant within each cycle). The approach can also be applied to other types of variable frequency control.

Acknowledgments

This research has been supported in part by the the Office of Naval Research under Multidisciplinary University Research Initiative (MURI) Grant N00014-96-1-1123, the U.S. Air Force Office of Scientific Research under Grant F49620-96-1-0161, and by a Senior Fulbright Scholar Award.

References

[1] C.-C. Fang and E.H. Abed, "Sampled-data modeling and analysis of PWM DC-DC converters I. Closed-loop circuits," preprint, Feb. 1998.

[2] C.-C. Fang and E.H. Abed, "Sampled-data modeling and analysis of PWM DC-DC converters II. The power stage," preprint, Feb. 1998.

[3] R. Redl and N.O. Sokal, "Current-mode control, five different types, used with the three basic classes of power converters: small-signal AC and classes large-signal DC characterization, stability requirements, and implementation of practical circuits," in *IEEE Power Electronics Specialists Conf. Rec.*, 1985, pp. 771–785.

[4] R Redl, "Small-signal high-frequency analysis of the free-running current-mode-controlled converter," in *IEEE Power Electronics Specialists Conf. Rec.*, 1991, pp. 897–906.

[5] Y.-F. Liu and P.C. Sen, "Large-signal modeling of hysteretic current-programmed converters," *IEEE Transactions on Power Electronics*, vol. 11, no. 3, pp. 423–430, 1996.

[6] C.-C. Fang, *Sampled-Data Analysis and Control of DC-DC Switching Converters*, Ph.D. thesis, University of Maryland, College Park, 1997.